

# Influence of free silica in the production of synthetic aggregates from bauxite residue

M. B. de Vilhena<sup>1\*</sup>, B. M. Viegas<sup>2</sup>, J. A. S. Souza<sup>1</sup>, E. N. Macêdo<sup>1</sup>

<sup>1</sup>Federal University of Pará, Graduate Program in Engineering of Natural Resources of the Amazon, 66075-110, Belém, PA, Brazil

<sup>2</sup>Federal University of Pará, Faculty of Biotechnology, 66075-110, Belém, PA, Brazil

## Abstract

The residue from the Bayer process has physicochemical characteristics that allow its use in the production of synthetic aggregate, although some characteristics such as low plasticity and water absorption still need better control. In this work, the influence of clay and silica addition on the sintering of synthetic aggregate produced from bauxite residue was analyzed. Compositions containing bauxite residue-sand-clay were elaborated, whose processing occurred using extrusion and crushing, followed by sintering at 1200 °C for 3 h. The X-ray diffraction analyses indicated the presence of new phases such as nepheline, originating from sodalite, and mullite resulting from the decomposition of kaolinite. Increasing the amount of free silica in the mixture resulted in an aggregate with a higher bulk density and lower water absorption, indicating that the amount of this raw material influenced the aggregate properties.

**Keywords:** bauxite residue, synthetic aggregate, sintering, silica, clay.

## INTRODUCTION

The increase in impacts on production has driven the interest in finding new ways to reuse waste materials [1], however, this reuse should be evaluated not only from the environmental point of view but also economically [2]. The main bauxite beneficiation step for the production of alumina ( $\text{Al}_2\text{O}_3$ ) is digestion with concentrated sodium hydroxide (NaOH) at high temperatures (up to 250 °C) and low pressures, which results in the formation of aluminate ions  $[\text{Al}(\text{OH})_4]^-$ , from gibbsite  $[\text{Al}(\text{OH})_3]$  and boehmite  $[\text{AlO}(\text{OH})]$ , and a solid material known as bauxite residue, composed mainly of iron oxides, quartz, sodium aluminosilicates, calcium carbonate, aluminates, titanium dioxide, and other metal oxides [3, 4]. This process is known as Bayer, being considered the most widely used method in the treatment of bauxite for alumina production [5]. Over 90% of the world's alumina production is produced through the Bayer process, and consequently, the generated bauxite residue represents a significant portion of by-products from alumina extraction [6]. For every one ton of alumina, on average 1.5 tons of bauxite waste are generated, and its global production exceeds 4 billion tons to the present day [7, 8]. Large amounts of bauxite waste produced in mining industries are not reused. Instead, they are stored in dams built on the surface taking up space and construction and maintenance costs [8, 9]. Research has been developed looking for a way to reduce the environmental impacts caused by bauxite waste [10-14].

The greatest complications are due to its high pH (caused by the presence of sodium hydroxide) and its large quantity [15]. Several disposal techniques and their compatibilities have been investigated worldwide, such as deep-sea dumping, landfilling, and storage in lagoons [16].

Since the 1950s, studies have been conducted to recover valuable components such as Fe, Al, Ti, and rare earth elements, present in bauxite residue through hydrometallurgical and pyrometallurgical methods. Besides these, there is also research on the use of the residue on a small scale in the manufacture of ceramic adsorbents, bricks, additives for high-performance concrete, and base materials for roads [17]. Different methodologies have already been developed for the production of synthetic aggregates, which generally consist of pelletizing granules between 0.5 and 20 mm in size, using different raw materials, such as gold mine tailings, limestone waste, coal acid leaching waste, fly ash, among others, to improve certain properties of the material depending on its application [18-21].

In this work, the production of synthetic aggregates from bauxite waste was evaluated in a mixture with clay and free silica, using a crushing and sintering process at 1200 °C for 3 h. The addition of sand as a source of free silica is an advantageous solution since it is a widely available material in nature and can provide desirable physical properties such as low water absorption. In addition, the inclusion of clay as a binding element is essential due to the low plasticity of bauxite waste. The crushing process used in this work enabled the production of aggregates with different granulometries and irregular shapes, in order to favor the aggregate-clay interaction and improve adhesion, besides reducing the amount of pores in the structure.

\*[mailson.vilhena@abaetetuba.ufpa.br](mailto:mailson.vilhena@abaetetuba.ufpa.br)

<https://orcid.org/0000-0003-0747-5845>

## MATERIALS AND METHODS

**Materials:** the raw materials used in the production of aggregates were bauxite residue from a mining company located in the Brazilian Amazon region, state of Pará, Brazil, construction sand (source of free silica), acquired from local commerce, and clay extracted from a mine located in the city of São Miguel do Guamá-PA, Brazil. The use of free silica in the composition aimed to promote better glass phase formation and consequent mullite phase formation ( $3\text{Al}_2\text{O}_3 \cdot 2\text{SiO}_2$ ), while the clay was used to provide plasticity to the mixture for better workability.

**Sample preparation:** initially, the deagglomeration of the raw materials was performed in a ball mill (Work Index) and dried in an air oven (SSDC-110L, SolidSteel) at 110 °C for 24 h. Subsequently, the clay was crushed in a jaw crusher (TE2, STM) and classified with a 60 mesh sieve (<60#) for particle size control. For a better use of the material, the sand was submitted to a milling process in a disk mill (MA700, Marconi). Finally, the raw materials were submitted to mixing following the proportions presented in Table I. Fig. 1 shows the raw materials after the sieving stage.

Table I - Proportion of each raw material for aggregate production.

Code	Bauxite residue (%)	Silica (%)	Clay (%)
S5	90	5	5
S15	80	15	5
S25	70	25	5

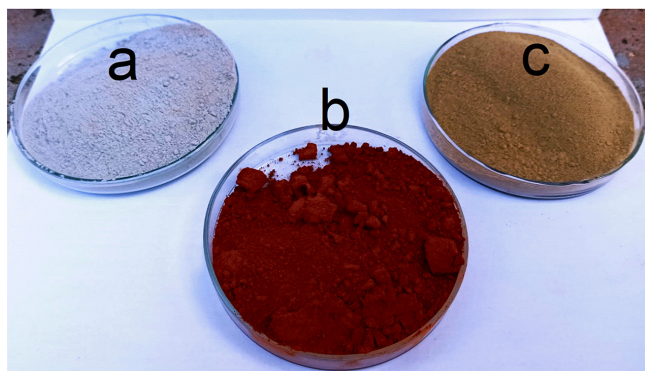


Figure 1: Photo showing the raw materials used: a) sand; b) bauxite residue; and c) clay.

**Production of the aggregates:** with the help of a mortar mixer (Solotest), about 25% water was added to form a paste, which was later extruded using equipment (Verdes) and cut into slabs (15x5x20 cm). Then, the slabs were dried in an air-circulating oven (SSDC-110L, SolidSteel) for 24 h and crushed (100 mm jaw opening). The crushed aggregates were sintered in an electric furnace (SSC, Jung) at 1200 °C with a heating rate of 10 °C/min for 3 h. A flowchart with the main steps of the aggregate production is presented in Fig. 2.

**X-ray diffraction (XRD):** mineralogical characterization of the samples was performed in a diffractometer (Empyrean,

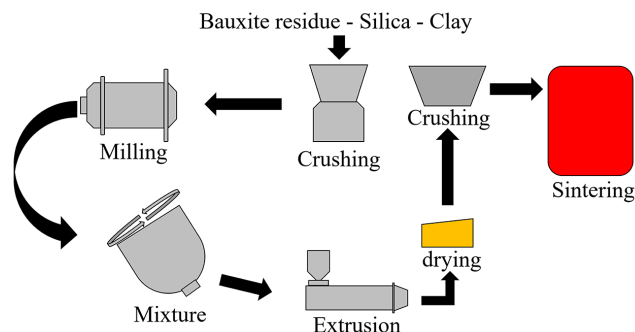


Figure 2: Flowchart to produce synthetic aggregates.

Panalitical) using Co anode ( $K\alpha_1=1.789010 \text{ \AA}$ ), long fine focus, FeK $\beta$  filter, PIXCEL3D-Medpix3 1x1 detector, in scanning mode, with a voltage of 40 kV, current of 35 mA, scanning from 3° to 75° of 2 $\theta$ , step size of 0.006° (2 $\theta$ ), and time/step of 20 s. The crystalline phases in the samples were identified and compared with the PDF files. **X-ray fluorescence spectroscopy (XRF):** the bauxite residue and clay were sorted on a 200 mesh sieve. They were then mixed with a binder (Cera Wax) at a ratio of 10 g of sample to 2 g of binder until completely homogenized and compacted. To identify the elements of interest, the sample aliquots were characterized by X-ray fluorescence spectroscopy using an equipment with XFlash detector (S2 Ranger, Bruker). **Scanning electron microscopy (SEM):** samples S25, S15, and S5 were analyzed using a scanning electron microscope (MIRA3, Tescan) operating at 17.5 kV. The sample preparation procedure consisted of mechanically breaking the aggregate and using sandpapers (200, 350, 600, and 1000 grit), polishing and flattening its surface. After sanding, the samples were submitted to an acid attack to remove the glassy phase, or part of it, to have a better visualization of the mullite phase, if it was formed during the sintering process. The acid used was the hydrofluoric acid in a 10% solution, in which the samples were immersed for 60 s and then washed with running water and dried in an oven with air circulation for a period of 24 h at 105 °C.

**Thermal analysis (thermogravimetry/differential scanning calorimetry, TG/DSC):** to evaluate the main reactions in the raw materials (bauxite-silica-clay residue), a thermal analysis was performed using an equipment (Nexta STA300, Hitachi) with the following operating conditions: temperature range of 25-1200 °C, heating rate of 10 °C/min and nitrogen atmosphere at a flow rate of 100 mL/min. **Bulk density/water absorption:** the sintered aggregates were submitted to tests to determine their bulk density and water absorption, whose procedures were based on ASTM C373-88:2006 standard [22], in which a precision balance (S2202H, Bel) with two decimal places of precision was used. Initially, 10 samples of each composition studied were measured. The calculation of the bulk density (BD) and water absorption (A) measurements were determined by:

$$BD = \frac{M_d}{M_w - M_s} \rho_{\text{water}} \quad (\text{A})$$

$$A = \frac{M_w - M_d}{M_d} 100 \quad (\text{B})$$

where  $\rho_{\text{water}}$  is the water density ( $1 \text{ g/cm}^3$ ),  $M_d$  is the dry mass,  $M_w$  is the saturated mass, and  $M_s$  is the immersed mass of the sample.

**RESULTS AND DISCUSSION**

Fig. 3 shows the aggregates before sintering (Fig. 3a) and after the process (Figs. 3b to 3d). It can be seen the effect of the addition of sand as a source of free silica by the coloration of



Figure 3: Image of the aggregates before sintering (a) and after the sintering of samples S5 (b), S15 (c), and S25 (d).

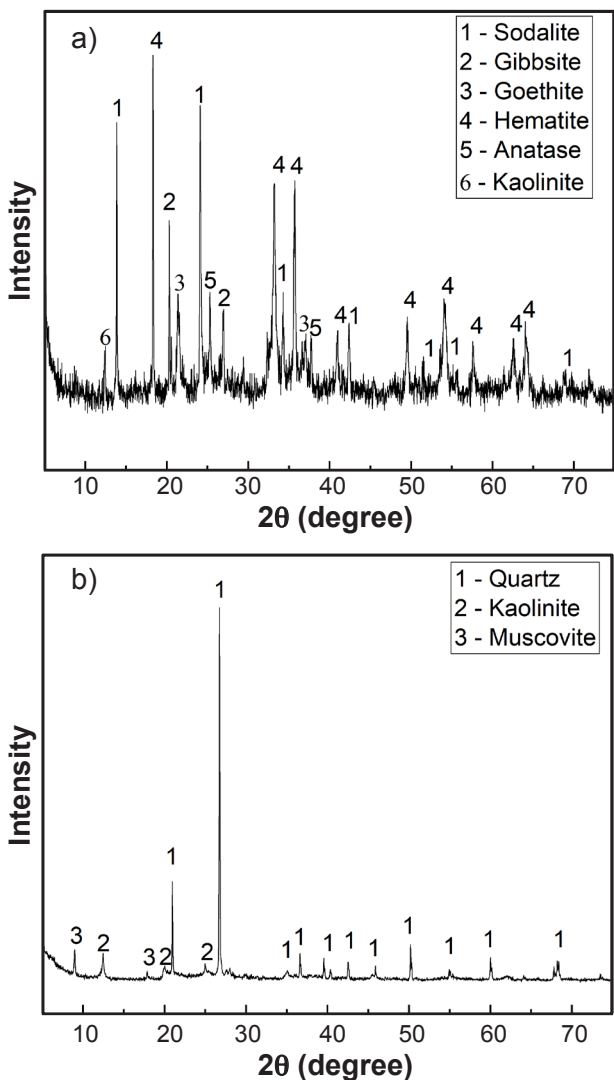


Figure 4: X-ray diffraction patterns of: a) bauxite residue; and b) clay.

Table II - Chemical composition (wt%) of bauxite residue and clay.

Oxide	Bauxite residue	Clay
Fe <sub>2</sub> O <sub>3</sub>	34.31	7.23
Al <sub>2</sub> O <sub>3</sub>	21.27	20.30
SiO <sub>2</sub>	17.72	65.50
Na <sub>2</sub> O	9.25	-
TiO <sub>2</sub>	6.89	1.71
CaO	1.22	0.12
ZrO <sub>2</sub>	-	0.11
K <sub>2</sub> O	-	2.67
MgO	-	1.74
LOI	8.11	-

LOI: loss on ignition.

the samples, because the silica promoted a greater formation of the glassy phase, resulting in the darkening of the samples. The glass phase is formed due to the reaction of the fluxing oxides and alkali metals present in bauxite residue with silicon oxide, whose results can be better observed in the internal part of the material that is highlighted in red in the figure. Regarding the morphology of the aggregates, it was decided to use crushing before being sintered. The irregular structure and the non-uniformity in the granulometry of these aggregates favor a better interaction with the cementitious mass in concrete applications, unlike what occurs in synthetic aggregates of spherical shape that form voids due to their structure, resulting in an increase in the consumption of cement and water. Another important factor is the surface roughness that enables a better interfacial mortar-aggregate interaction and can improve the mechanical performance of concrete.

The results of the X-ray diffraction analysis of the bauxite residue and the clay are presented in Figs. 4a and 4b, respectively. In the analysis of the bauxite residue, it was

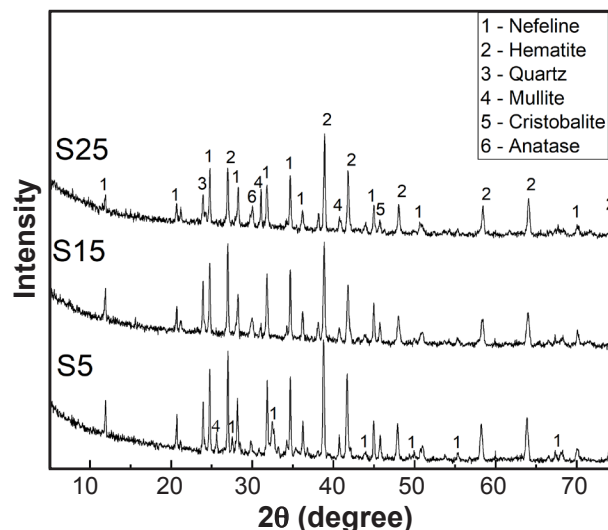


Figure 5: X-ray diffraction patterns of the S5, S15, and S25 aggregates after sintering at 1200 °C.

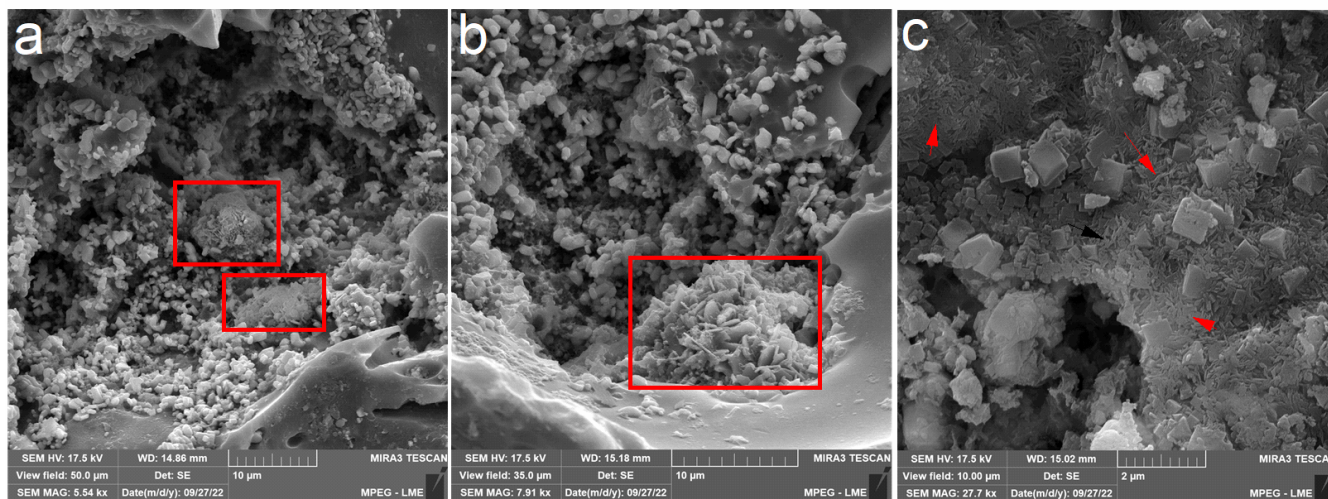


Figure 6: Scanning electron micrographs of the aggregates after sintering at 1200 °C: a) S25; b) S15; and c) S5 (surfaces etched with HF).

possible to identify the following mineral phases: sodalite ( $\text{Na}_2\text{O}\cdot\text{Al}_2\text{O}_3\cdot\text{SiO}_2$ , PDF 96-900-5053); gibbsite [ $\text{Al}(\text{OH})_3$ , PDF 96-154-4376], goethite [ $\text{FeO}(\text{OH})$ , PDF 96-901-0411]; hematite ( $\text{Fe}_2\text{O}_3$ , PDF 96-900-9783); anatase ( $\text{TiO}_2$ , PDF 96-720-6076); and kaolinite [ $\text{Al}_2\text{Si}_2\text{O}_5(\text{OH})_4$ , PDF 96-900-9235]. Three mineral phases were identified in the clay: quartz ( $\text{SiO}_2$ , PDF 96-101-1177), kaolinite [ $\text{Al}_2\text{Si}_2\text{O}_5(\text{OH})_4$ , PDF 96-900-9235], and muscovite [ $\text{KAl}_2\text{Si}_2\text{O}_5(\text{OH})_4$ , PDF 96-101-1050]. Table II shows the chemical composition of bauxite residue, whose presented oxides of iron, aluminum, silicon, sodium, titanium, and calcium. The physical, chemical, and mineralogical properties of bauxite residue can vary according to the source of bauxite and the process used in its beneficiation [23]. It was observed that the clay used in this work was composed mostly of silica (65.5% by weight) and alumina (20.3% by weight) followed by other oxides in smaller quantities.

Fig. 5 shows the X-ray diffraction results of samples S5, S15, and S25 after undergoing the sintering process. The phases identified in the three samples were nepheline (PDF 96-400-2836), hematite (PDF 96-900-9783), quartz (PDF 96-900-5025), mullite (PDF 96-900-1622), cristobalite (PDF 96-901-6250), and anatase (PDF 96-101-0943). The nepheline is a feldspathoid that occurs in nature in intrusive and volcanic rocks with low silica content [24]. The latter acts as an inhibitor for its formation [25], which may justify the reduction in the intensity of its characteristic peaks as the amount of free silica in the sample composition was increased. Crystallization in nepheline glasses occurs through a sequence of transformations that strongly depend on the chemical composition of the material. In bauxite residue, nepheline is formed due to the presence of sodium and silicon, which are precursors in the formation of species like  $\text{Na}_3\text{Al}_3\text{O}_{15}$  [26]. Oxides like  $\text{TiO}_2$  and  $\text{Fe}_2\text{O}_3$  favor nucleation to obtain nepheline crystals [24]. The presence of the mullite and cristobalite phases observed in Fig. 5 arose from the thermal decomposition of kaolinite [27]. The crystallization temperature of mullite observed in bauxite

residue was lower than that observed in other materials reported in the literature (>1300 °C [27]). This phenomenon can be attributed to the alkali metal oxides present in bauxite residue that assist the sintering process by reducing the softening temperature of the liquid phase and the reaction temperature [28]. The hematite and anatase phases present in both bauxite residue (Fig. 4a) and aggregates (Fig. 5) were stable [29] and did not undergo transformations during the sintering process. In order to confirm the effect of the presence of free silica in the formation of mullite in the aggregate produced, SEM analyses were performed as shown in Fig. 6. It is observed in the micrographs the presence of mullite (elongated shape) in all samples (areas highlighted in red). The morphology of mullite crystals depends not only on the amount of liquid formed but also on the sintering temperature since the reaction between alumina and quartz is controlled by a dissolution-precipitation mechanism [30].

In Fig. 7 the thermal behaviors of bauxite residue and compositions S5, S15, and S25 are presented. The temperature ranges of the main events were identified through DSC analysis. The mass loss in the first temperature range (50-230 °C) can be attributed to the loss of water absorbed by the particle and the decomposition of gibbsite. In the range 230-700 °C, goethite decomposition with the formation of hematite, decarbonation of calcite [31], and transition from quartz- $\alpha$  to quartz- $\beta$  [32, 33] occurred. Between 700-1200 °C, there was decomposition of volatile species trapped inside the sodalite structure [31]. It was also observed a shift in the TG curve as silica was added that may be associated with the percentage reduction of bauxite residue in the composition. In the sample with 100% bauxite residue, there was a total mass loss of 12.81%, and in the composition S25 (70% bauxite residue), this loss was reduced to 9.33%. In the DSC curve, the first endothermic peak at approximately 90 °C was associated with the evaporation of water absorbed by the material. The peak at 173.86 °C may be associated with the dehydration of gibbsite [34]. The peak at 267.41 °C was due to the decomposition of gibbsite to form a transition

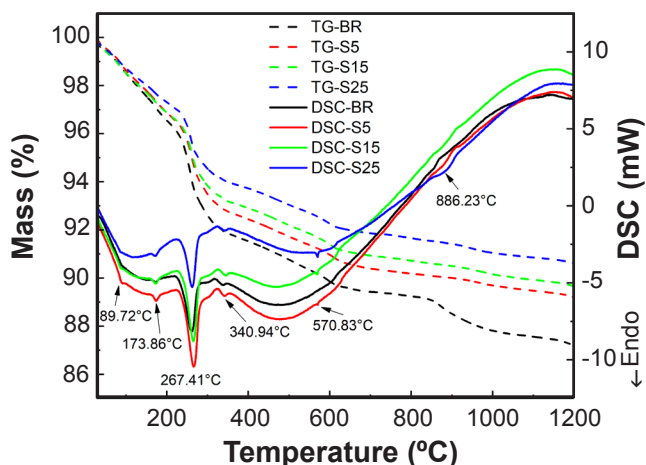


Figure 7: TG and DSC curves of bauxite residue (BR) and compositions S5, S15 and S25.

Table III - Bulk density and water absorption results for samples S5, S15, and S25.

Sample	Bulk density (g/cm <sup>3</sup> )	Absorption (%)
S25	2.19±0.20	2.60
S15	2.30±0.26	8.12
S5	1.89±0.18	11.35

alumina ( $\chi$ -Al<sub>2</sub>O<sub>3</sub>) [34, 35]. The peaks at 340 °C may be related to the decomposition of goethite to the formation of hematite [34, 35], at 570 °C the calcite decomposition [31, 36], which may also be associated with the transformation from quartz- $\alpha$  to quartz- $\beta$  [32, 33], and at 886.23 °C may be associated with nepheline formation [31, 36].

Table III shows the results of bulk density and water absorption of the produced aggregates. The bulk density of sample S5 was 1.89 g/cm<sup>3</sup>, due to the little formation of the glassy phase that was associated with a low amount of silica in its composition. On the other hand, as the amount of silica increased, the bulk density increased to values higher than 2 g/cm<sup>3</sup>. It can also be seen that the percentage of water absorption decreased as silica was added to the composition. The absorption rate reflects the sintering degree, i.e., the lower the absorption rate, the higher the sintering degree [37].

## CONCLUSIONS

The results obtained in this work showed that it was possible to obtain synthetic aggregates with interesting characteristics by using bauxite residue combined with other materials such as clay and sand. It was verified through the analyses of bulk density and water absorption that the addition of sand modified the physical properties of the material. The X-ray diffraction results revealed that the intensity of the nepheline phase peaks reduced as sand was added to the material composition. Some phases such as hematite and anatase remained stable and did not undergo phase transformations after sintering. The mullite

phase was formed in all samples and its elongated structures were detected by scanning electron microscopy. Through thermal analysis, it was possible to observe the main events of phase transformation and their respective mass losses. It was noticeable in the thermogravimetry analysis the reduction of mass loss with the addition of sand. The clay is an excellent binder and enabled a better conformation of the pellets during the aggregate production process, and the addition of sand contributed to the formation of mullite and to the densification of the aggregate, significantly reducing water absorption. In terms of processing, crushing proved to be an innovative way for larger-scale production, as well as to improve the physical characteristics of the material. The use of bauxite residue in a mixture with sand and clay proved to be an alternative proposal to natural aggregates. Therefore, the use of bauxite residue combined with other materials of great abundance in nature in the formation of synthetic aggregates proved to be a plausible way to reuse large volumes of waste in the production of aggregates with interesting characteristics that can be used in the production of concrete for civil construction, considering that the composition of these aggregates can reach 90% of bauxite residue, as in sample S5 (with 5% sand and 5% clay).

## ACKNOWLEDGMENTS

The authors thank the office for research National Council for Scientific and Technological Development (CNPq, Brazil) and Coordination for the Improvement of Higher Education Personnel (CAPES, Brazil) for their financial support.

## REFERENCES

- [1] P. Tataranni, G.M. Besemer, V. Bortolotti, C. Sangiorgi, *Materials* **11**, 7 (2018) 1255.
- [2] A.J.M. Araujo, H.P.A. Alves, R.M. Andrade, L.F.A. Campos, D.A. Macedo, A.L.S. Pinho, R.M. Nascimento, C.A. Paskocimas, *Ceram. Int.* **45**, 7 (2019) 8525.
- [3] A. Occhicone, M. Vukčević, I. Bosković, C. Ferone, *Sustainability* **13**, 20 (2021) 11298.
- [4] E.M. Magalhães, E.N. Macêdo, D.D. Quaresma, J.A.S. Souza, J.N. Quaresma, in *EPD Congress*, John Wiley Sons (2012) 345.
- [5] Y. Zhan, R. Xu, H. Tang, L. Wang, W. Sun, *J. Hazard. Mater.* **397** (2020) 122772.
- [6] Y. Wang, T. Zang, G. Lyu, F. Guo, W. Zhang, Y. Zhang, *J. Clean. Prod.* **188** (2018) 456.
- [7] S. Alam, S.K. Das, B.H. Rao, *Constr. Build. Mater.* **211** (2019) 932.
- [8] P. Liu, G. Shao, R. Huang, *Am. Soc. Civil Eng.* **33**, 5 (2019) 1.
- [9] R. Chen, G. Cai, X. Dong, D. Mi, A.J. Puppala, W. Duan, *Constr. Build. Mater.* **216** (2019) 188.
- [10] C.R. Borra, B. Blanpain, Y. Pontikes, K. Binnemans, T. Van Gerven, *J. Sustain. Metall.* **2** (2016) 365.
- [11] K. Binnemans, P.T. Jones, B. Blanpain, T. Van Gerven,

- Y. Pontikes, *J. Clean. Prod.* **99** (2015) 17.
- [12] W. Liu, X. Chen, W. Li, Y. Yu, K. Yan, *J. Clean. Prod.* **84** (2014) 606.
- [13] É. Ujaczki, V. Feigl, M. Molnár, P. Cusack, T. Curtin, R. Courtney, L. O'Donoghue, P. Davris, C. Hugi, M.W.H. Evangelou, E. Balomenos, M. Lens, *J. Chem. Technol. Biotechnol.* **93**, 9 (2018) 2498.
- [14] Z. Liu, H. Li, *Hydrometallurgy* **155** (2015) 29.
- [15] D. Winkler, A. Bidló, B. Bolodár-Varga, Á. Erdő, A. Horváth, *Sci. Total Environ.* **644** (2018) 1292.
- [16] M.A. Khairul, J. Zanganeh, B. Moghtader, *Resour. Conserv. Recycl.* **141** (2019) 483.
- [17] G. Wang, C. Zhang, W. Wang, S. Wu, J. Li, X. Wang, C. Wu, *Materials* **14**, 1 (2021) 218.
- [18] F. Andreola, I. Lancellotti, R. Sergi, V. Cannillo, L. Barbieri, *Materials* **14**, 1 (2021) 167.
- [19] W.J. Ju, D. Shin, H. Park, K. Naum, *Metals* **7**, 10 (2017) 390.
- [20] C. Song, H. Zhang, Y. Dong, L. Pei, H. Liu, J. Jiang, H. Xu, *Chin. J. Chem. Eng.* **32** (2021) 353.
- [21] K. Tian, Y. Wang, S. Hong, J. Zhang, D. Hou, B. Dong, F. Xing, *Constr. Build. Mater.* **281** (2021) 122552.
- [22] ASTM, C373-88, "Standard test method for water absorption, bulk density, apparent porosity, and apparent specific gravity of fired whiteware products", ASTM Int., USA (2006).
- [23] M.L.P. Antunes, S.J. Couperthwaite, F.T. da Conceição, C.P.C. de Jesus, P.K. Kiyohara, A.C.V. Coelho, R.L. Frost, *Ind. Eng. Chem. Res.* **51**, 2 (2012) 775.
- [24] A. Deshkar, M. Ahmadzadeh, A. Scrimshire, E. Han, P.A. Bingham, D. Guillen, J. McCloy, A. Goel, *J. Am. Ceram. Soc.* **102**, 3 (2019) 1101.
- [25] I. Sargin, C.E. Lonergan, J.D. Vienna, J.S. McCloy, S.P. Beckman, *J. Am. Ceram. Soc.* **103**, 9 (2020) 4913.
- [26] B.M. Viegas, E.M. Magalhães, J.A.S. Souza, E.N. Macêdo, *Matéria* **25**, 1 (2020) e12594.
- [27] P.J. Sánchez-Soto, D. Eliche-Quesada, S. Martínez-Martínez, E. Garzón-Garzón, L. Pérez-Villarejo, J.M. Rincón, *Mater. Lett.* **223** (2018) 154.
- [28] W. Wang, W. Chen, H. Liu, *Ceram. Int.* **45**, 8 (2019) 9852.
- [29] B.M. Viegas, E.M. Magalhães, H.R.B. Orlande, D.C. Estumano, E.N. Macêdo, *Int. J. Environ. Sci. Technol.* **20** (2023) 5533.
- [30] Z. Hou, C. Liu, L. Liu, S. Zhang, *Ceram. Int.* **44**, 15 (2018) 17914.
- [31] J.M. Rivas Mercury, A.A. Cabral, A.E.M. Paiva, R.S. Angelica, R.F. Neves, T. Scheller, *J. Therm. Anal. Calorim.* **104**, 2 (2011) 635.
- [32] A.H.A. Pereira, D.Y. Miyaji, M.D. Cabrelon, J. Medeiros, J.A. Rodrigues, *Cerâmica* **60**, 355 (2014) 449.
- [33] S. Bakhtiyari, A. Allahverdi, M. Rais-Ghasemi, B.A. Zarrabi, T. Parhizkar, *Thermochim. Acta* **514**, 1-2 (2011) 74.
- [34] S. Samal, A.K. Ray, A. Bandopadhyay, *J. Clean. Prod.* **101** (2015) 368.
- [35] A. Atasoy, *J. Therm. Anal. Calorim.* **90**, 1 (2007) 153.
- [36] H. He, Q. Yue, Y. Qi, B. Gao, Y. Zhao, H. Yu, J. Li, Q. Li, Y. Wang, *Appl. Clay Sci.* **70** (2012) 67.
- [37] C. Song, H. Zhang, Y. Dong, L. Pei, H. Liu, J. Jiang, H. Xu, *Chin. J. Chem. Eng.* **32** (2021) 353.
- (*Rec.* 02/05/2023, *Rev.* 23/06/2023, 03/07/2023, *Ac.* 10/07/2023)